

## PREDICTION OF PROPELLER FORCES DURING SHIP MANEUVERING

TOMASZ ABRAMOWSKI

*Faculty of Maritime Technology, Technical University of Szczecin*

*e-mail: tomasz.abramowski@ps.pl*

A method is proposed for the determination of propeller forces during ship maneuvering. Artificial neural networks were applied to the performance prediction of a propeller working under such conditions as braking, stopping and running astern. Furthermore, an effect of oblique motion of a maneuvering ship, is studied by means of computational fluid dynamics methods. Wake distributions in the propeller plane are presented when the drift angle gets higher. A simple application example of the discussed methods is presented for a real case of a maneuvering ship.

*Key words:* ship manoeuvring, ship propeller forces

### 1. Introduction

A lot of attention has been given recently to the safety of sea traffic. Ship maneuvering is an important subject of these investigations, increasing the interest in numerical maneuvering simulators. Such interest increases the requirements for models applied in simulators. While they are presently a well recognized tool for the determination of ship maneuvering qualities in design phase as well as for the training of crew members, there are still many areas where additional research is purposeful. In the present work, we have focused on the performance of propellers during maneuvering, mainly affected by such conditions as braking, stopping, running astern and moving with drift. Simulation of a maneuvering ship is based on solutions of differential equations describing her motions as a function of hydrodynamic forces, such as wind or wave forces, rudder forces or propeller forces. As the maneuvering simulation covers 3DOF motion in the plane of water, we are interested in the prediction of two propeller forces: the thrust  $T$  (ship longitudinal direction, propelling

force) and the side force  $Y$ , resulting from oblique or rotational motion of a ship. Furthermore, for the purposes of the coupling the propeller revolutions and the dynamics of ship's propulsion machinery, the propeller torque  $Q$  should be predicted as well. All these forces and torque can be written in the following form

$$\begin{aligned} T &= K_T(J)\rho D^4 n^2 \\ Q &= K_Q(J)\rho D^5 n^2 \\ Y &= K_Y(J)\rho D^4 n^2 \end{aligned} \quad (1.1)$$

In the above equations  $\rho$  is the density of water,  $D$  is the propeller diameter and  $n$  is the number of propeller revolutions.  $K_T$ ,  $K_Q$  and  $K_Y$  are hydrodynamic coefficients being the functions of the advance coefficient  $J$

$$J = \frac{V_A}{nD} = \frac{V(1-w)}{nD} \quad (1.2)$$

where  $V_A$  indicates the propeller inflow velocity,  $V$  is ship's speed and  $w$  is the effective wake factor describing the hull-propeller interaction. For the prediction of propeller forces and torque, it is necessary to determine at first the hydrodynamic coefficients  $K_T$ ,  $K_Q$  and effective wake factor  $w$ . For the determination of the side force  $Y$ , there is a number of empirical or semi-empirical relationships, where the side force  $Y$  is given as a function of  $K_T$  or  $K_Q$  coefficients and the transverse component of the mean water velocity in the propeller plane. For the analysis carried out in the present work, the following formula has been adopted (Weinicki, 1966)

$$Y = 2\rho n D^3 V_y K_Q(J) \quad (1.3)$$

where  $K_Q(J)$  is the torque coefficient and  $V_y$  is the transverse component of the mean water velocity in the propeller plane. The above considerations lead to the conclusion that for accurate prediction of propeller forces and torque we must determine propeller hydrodynamic characteristics, i.e. functions of  $K_T(J)K_Q(J)$  in all possible conditions such as braking, stopping and running astern. Furthermore, the propeller inflow velocity field has to be known for the case when a ship is moving with a drift angle (oblique inflow), as it takes place during manoeuvring. Present methods for the determination of propeller forces during maneuvering operations are still mainly based on model tests results. Such methods are usually time and cost consuming when compared with numerical or modern regression analysis methods. The authors like Inoue *et al.* (1981), Kijama *et al.* (1993) and Kobylński and Zolfaghari (1997)

present results of simulations with experimentally derived thrust and wake factors. Attempts have also been made to assess hydrodynamic phenomena in the stern region of a maneuvering ship. Simonsen (2000) carried out calculations of separated configurations of the rudder, rudder behind a propeller and bare hull moving straight ahead without drift. He applied RANS equations with the Baldwin-Lomax turbulence model. Le Thuy Hang (2001) presented analysis of the propeller-rudder interaction with the lifting surface theory applied. Yosukuawa *et al.* (1996) have developed an algorithm for calculations of forces acting on a ship and hull-propeller interaction coefficients. The method is almost purely theoretical, but the wake factor  $w$  is obtained experimentally. El Moctar (2001) applies a finite volume method to viscous flow calculations of a ship hull. The results of hull forces are presented as a function of drift angles.

In the present work, artificial neural networks have been applied for the determination of propeller performance under conditions of braking, stopping and running astern (so-called "four-quadrant characteristics" or "off-design" characteristics). The problem of oblique propeller inflow velocity has been solved by means of computational fluid dynamics techniques. The Fluent Inc. solver has been applied for the analysis. Furthermore, an application example of the discussed methods is presented for a real case of a maneuvering ship.

## 2. Application of neural networks for the determination of propeller performance in four-quadrants

Apart from the normal operational state, which is propelling the ship in the ahead direction, marine propellers must also operate under conditions of braking and stopping in both ahead and astern directions. These conditions include states defined by the propeller inflow velocity  $V_A$  and the direction of rotation  $n$ . Thrust and torque coefficients  $K_T$  and  $K_Q$  are given as a function of the advance coefficient  $J$ , where  $K_T$ ,  $K_Q$  and  $J$  can achieve negative values. In this representation, the four quadrants are defined as: ahead  $(+V_A, +n)$ ; crash-ahead  $(-V_A, +n)$ ; crash-back  $(+V_A, -n)$  and backing  $(-V_A, -n)$ , see Fig. 1. In ahead and backing conditions,  $K_T$  and  $K_Q$  can achieve both positive and negative values while crash-ahead values are only positive, and those for crash-back are negative.

Use of Artificial Neural Networks (ANNs) for this purpose seems to be attractive because of its capability for data storage, interpolation and some extrapolation. ANNs are more effective than conventional regression analysis

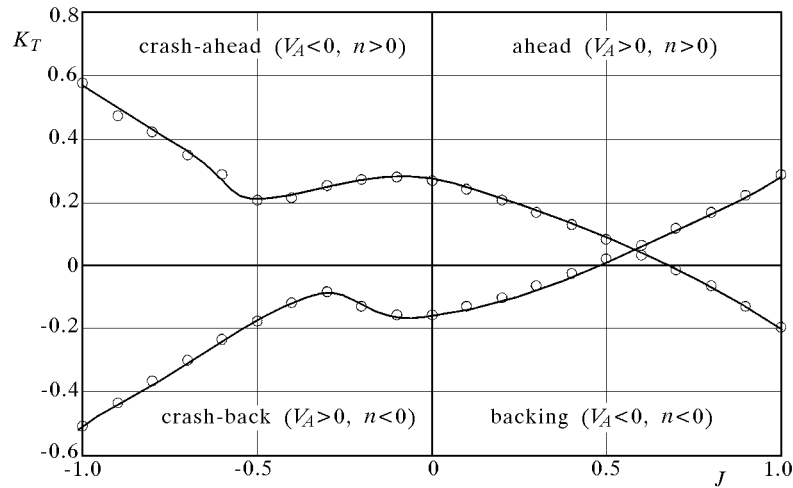


Fig. 1.  $K_T$  as a function of the advance coefficient (four-quadrant representation)

methods, especially for noisy data. The learning and testing data set was taken mostly from Basin and Miniovich (1963), Chen and Stern (1999), Lammeren *et al.* (1969). Propeller crash-back, crash-ahead and backing conditions were the subjects of investigation. The structure of a neural network consists of a number of processing units that communicate with each other by sending signals. The idea of ANNs comes from biological neural structures, and its computations are similar to those the human brain regularly performs. Krose and Smagt (1996), give good introductions to the topic for readers not familiar with the basics of neural networks. The basic structure of an ANNs consists of:

- input layer – feeding the network with input data;
- hidden layers – the processing units. Hidden layers are made of single neurons whose connections transmit and process the signal in a way corresponding to an activation function used. Typical activation functions are linear, sigmoid, bipolar, and threshold functions;
- output layer – sending data out of the network. Usually the output layer also acts as a hidden layer.

Figure 2 shows an example of the ANN structure. The network presented there has two inputs, one hidden layer with four neurons and two outputs. The purpose of the learning process is to calculate values of weights and biases and then keep them for use in the network. After the learning process, equations of linear algebra are used, Eq. (2.1), to calculate output values for given input values. Here, the equation is given for the network structure as presented in

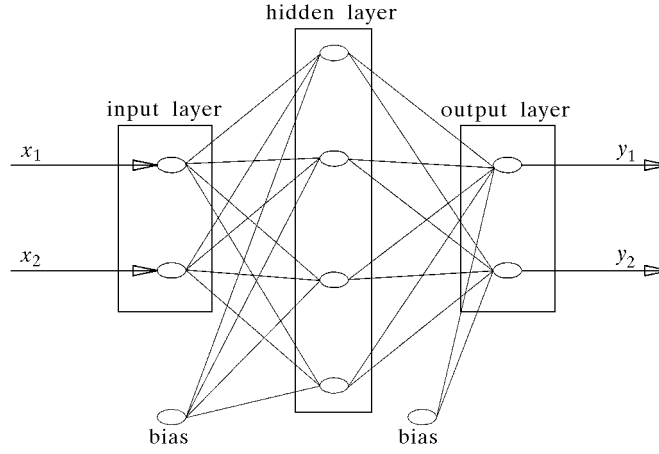


Fig. 2. An example of a neural network structure

Fig. 2. A typical procedure for training the network is *back-propagation method* in which the network starts with a randomly chosen set of weights. The output is compared to the input, and the error is calculated and propagated back within the network connections. Then new, hopefully better, values of weights are calculated

$$y_i = FO_i \left[ \sum_{k=1}^4 FH_k \left( \sum_{l=1}^2 x_l WH_{l,k} + W_{BH,k} \right) WO_{i,k} + W_{BO,i} \right] \quad (2.1)$$

$FO_i$  are output functions,  $FH_k$  are hidden layer functions,  $WH_{k,l}$  are weights of connections between the input and hidden layer,  $WO_{i,k}$  are weights of connections between the hidden and output layers,  $W_{BH}$  and  $W_{BO}$  are bias values,  $l$  is a number of inputs,  $k$  is a number of neurons in the hidden layer,  $i$  is a number of outputs. The selection of the network structure, topology, training method and activation functions is a trial-and-error task. It varies according to the application, data type and number of inputs/outputs. It is necessary to test different structures and control their behavior strictly during the learning process. A total of 30 screw propeller models were selected for the analysis. Their geometry parameters varied as follows:

- number of blades  $Z$  – from 3 to 5
- blade area ratio  $A_E/A_0$  – from 0.45 to 1.1
- pitch ratio  $P/D$  – from 0.6 to 1.8.

Due to a very limited set of screw models tested, it would be difficult to design a network producing acceptable results and having screw geometry parameters as arguments. Instead of this, an other approach is proposed here. It assumes that the first quadrant characteristic (ahead condition) represents the screw propeller geometry parameters, and can be used as the input to an ANN. The ahead condition performance can be obtained much easier than for the other quadrants. For most propellers, the given first quadrant performance can be approximated with sufficient accuracy by a second-degree polynomial of the form

$$K_T, K_Q = A_1(J)^2 + A_2(J) + A_3 \quad (2.2)$$

The outputs are functions of crash-back, crash-ahead and backing conditions. For crash-back and crash-ahead, the outputs cover the most critical range of  $K_T$  and  $K_Q$  discrete values for advance coefficients  $J$  starting from  $-0,1$  to  $-0,8$ . For the backing condition, the second-degree polynomial approximation can be used again, and the outputs are three coefficients  $A_{1b}, A_{2b}, A_{3b}$  similar to these in Eq. (2.2). The initial analysis showed that three partial ANNs designed for crash back, crash-ahead and backing conditions separately yield a better result than using only one for all. Thus, each ANN has three inputs (arguments), namely the coefficients  $A_1, A_2, A_3$ . Such a representation is a data compression problem for which ANNs have been successfully used (Osowski, 1996). The information on structures of partial networks was summarized in Table 1.

**Table 1.** Structures of designed networks

Condition	ANN structure	Inputs	Outputs
crash-ahead	$3 \times 5 \times 8$	$A_1, A_2, A_3$	Discrete values $K_T, K_Q(J = -0.1, -0.2, \dots, -0.8)$
crash-back	$3 \times 5 \times 8$	$A_1, A_2, A_3$	Discrete values $K_T, K_Q(J = -0.1, -0.2, \dots, -0.8)$
backing	$3 \times 4 \times 3$	$A_1, A_2, A_3$	$A_{1b}, A_{2b}, A_{3b}$ polynomial coefficients

The *back propagation* learning rule was applied for the training networks. As the bipolar activation function showed the best performance during the optimization process, it was applied to all partial networks. The bipolar function has the form

$$B_p(u) = \frac{2}{1 + e^{-u}} - 1 \tag{2.3}$$

where  $u$  is the input signal.

For example, for the prediction of  $K_T$  values in the crash-ahead condition, the learning rate value (constant of proportionality, expressing the training performance) was 0.22. The momentum constant, which determines the effect of the previous weight change, was 0.3. An example of application and verification is presented on the basis of DTNSRDC 4381 series propeller. Figure 3 presents the four-quadrant performance produced by the ANN by means of the above method. The agreement with experimental data is reasonably good. Statistical estimation of such an approximation was carried out on the basis of the correlation coefficient calculated for all quadrants. Results of this assessment are presented in Table 2. The mean square error given in the second column of the table is a target function applied as a parameter for the learning process quality assessment. It is calculated as a sum of errors of all pairs in the learning set.

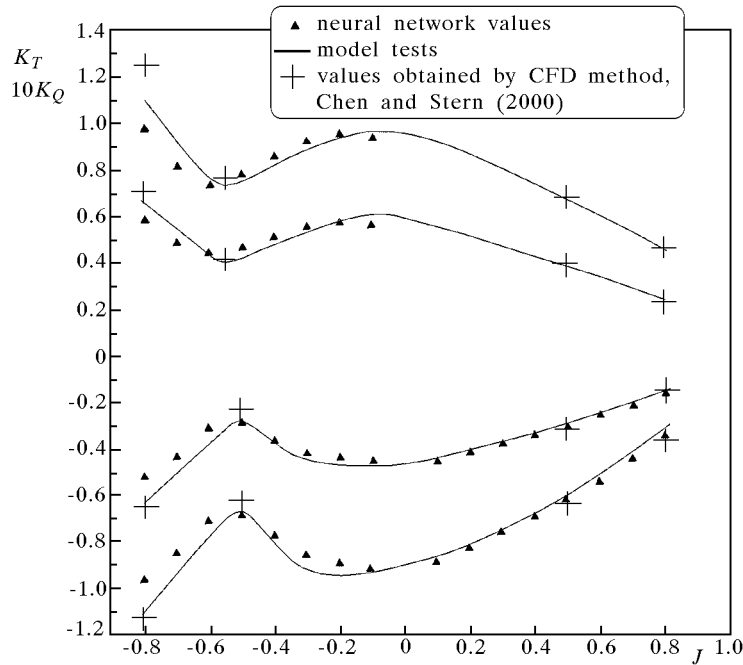


Fig. 3. Four-quadrant performance of the DTNSRDC 4381 propeller produced by a neural network in comparison with model tests and CFD method

**Table 2.** Statistical assesment of obtained results

	Curvilinear correlation coeff.	Mean square error
$K_T$ crash-ahead	0.87	0.025
$K_T$ crash-back	0.91	0.020
$K_T$ backing	0.99	0.018
$K_Q$ crash-ahead	0.84	0.004
$K_Q$ crash-back	0.94	0.002
$K_Q$ backing	0.99	0.002
Mean correlation coeff.	0.92	

The method presents good correlation with experimental data and it is purposeful for practical use to propose empirical formulae based on trained ANNs. All of the equations presented below have a matrix form, as the approach was multiple input and multiple output. For crash-ahead and crash-back conditions, we get the following equation

$$\begin{bmatrix} K_T & K_{Q(J=-0.8)} \\ K_T & K_{Q(J=-0.7)} \\ K_T & K_{Q(J=-0.6)} \\ K_T & K_{Q(J=-0.5)} \\ K_T & K_{Q(J=-0.4)} \\ K_T & K_{Q(J=-0.3)} \\ K_T & K_{Q(J=-0.2)} \\ K_T & K_{Q(J=-0.1)} \end{bmatrix} = B_p \left\{ \mathbf{W}_2 \times \left\{ B_p \left[ \left( \mathbf{W}_1 \times \begin{bmatrix} A_3 \\ A_2 \\ A_1 \end{bmatrix} \right) + \mathbf{B}_1 \right] \right\} + \mathbf{B}_2 \right\} \quad (2.4)$$

where  $B_p$  is the bipolar activation function used, Eq. (2.3), the input vector is a one-column matrix with the coefficients  $A_1, A_2, A_3$  in Eq. (2.2). Thus, for the application of presented formulae first quadrant curve of  $K_T, K_Q$  must be approximated with Eq. (2.2), e.g. by means of the least-square method.  $\mathbf{W}_1, \mathbf{W}_2$  are matrices of weight values,  $\mathbf{B}_1, \mathbf{B}_2$  are matrices of bias values. For the backing condition, the formulae can be written as

$$\begin{bmatrix} A_{3b} \\ A_{2b} \\ A_{1b} \end{bmatrix} = B_p \left\{ \mathbf{W}_2 \times \left\{ B_p \left[ \left( \mathbf{W}_1 \times \begin{bmatrix} A_3 \\ A_2 \\ A_1 \end{bmatrix} \right) + \mathbf{B}_1 \right] \right\} + \mathbf{B}_2 \right\} \quad (2.5)$$

The input vector is the same as for the crash-ahead and crash-back conditions, the output is a vector consisting of second-degree polynomial coefficients,  $(A_{3b}, A_{2b}, A_{1b})$  approximating  $K_T$  and  $K_Q$  values as a function of the advance coefficient identical to Eq. (2.5). Values of  $\mathbf{W}_1, \mathbf{W}_2, \mathbf{B}_1, \mathbf{B}_2$  matrices can be found in Abramowski (2003).

### 3. Numerical wake assessment of maneuvering ship

Apart from values of  $K_T$  and  $K_Q$ , wake characteristics of a maneuvering ship must be further determined. They describe the propeller-hull interaction, and the nominal wake factor  $w_N$ , calculated here, represents the influence of a bare hull and does not take the propeller action into consideration. For the calculation of viscous flow around a bare ship hull without a propeller with drift we have applied a numerical method based on solving equations holding for the case under consideration, i.e. RANS equations. These equations have the following form for the incompressible steady flow

$$\begin{aligned}
 \rho \left( u \frac{\partial u}{\partial x} + v \frac{\partial u}{\partial y} + w \frac{\partial u}{\partial z} \right) \rho &= F_1 - \frac{\partial P}{\partial x} + \mu \left( \frac{\partial^2 u}{\partial x^2} + \frac{\partial^2 u}{\partial y^2} + \frac{\partial^2 u}{\partial z^2} \right) - \\
 &\quad - \rho \left( \frac{\partial \overline{u'u'}}{\partial x} + \frac{\partial \overline{u'v'}}{\partial y} + \frac{\partial \overline{u'w'}}{\partial z} \right) \\
 \rho \left( u \frac{\partial v}{\partial x} + v \frac{\partial v}{\partial y} + w \frac{\partial v}{\partial z} \right) \rho &= F_2 - \frac{\partial P}{\partial y} + \mu \left( \frac{\partial^2 v}{\partial x^2} + \frac{\partial^2 v}{\partial y^2} + \frac{\partial^2 v}{\partial z^2} \right) - \\
 &\quad - \rho \left( \frac{\partial \overline{u'v'}}{\partial x} + \frac{\partial \overline{v'v'}}{\partial y} + \frac{\partial \overline{v'w'}}{\partial z} \right) \\
 \rho \left( u \frac{\partial w}{\partial x} + v \frac{\partial w}{\partial y} + w \frac{\partial w}{\partial z} \right) \rho &= F_3 - \frac{\partial P}{\partial z} + \mu \left( \frac{\partial^2 w}{\partial x^2} + \frac{\partial^2 w}{\partial y^2} + \frac{\partial^2 w}{\partial z^2} \right) - \\
 &\quad - \rho \left( \frac{\partial \overline{u'w'}}{\partial x} + \frac{\partial \overline{v'w'}}{\partial y} + \frac{\partial \overline{w'w'}}{\partial z} \right)
 \end{aligned} \tag{3.1}$$

In the above equations,  $u$ ,  $v$ ,  $w$  are components of the mean velocity vector,  $P$  is the pressure,  $\mu$  is the viscosity,  $u'$ ,  $v'$ ,  $w'$  are fluctuation parts of the velocity vector,  $F_1$ ,  $F_2$ ,  $F_3$  are volumetric forces. Furthermore, the model must satisfy continuity equation

$$\frac{\partial u}{\partial x} + \frac{\partial v}{\partial y} + \frac{\partial w}{\partial z} = 0 \tag{3.2}$$

The RNG  $k - \varepsilon$  turbulence model has been applied for modelling of the Reynolds stresses. The algorithm is based on the finite volume method with second-order approximations. The SIMPLE algorithm is employed for the coupling of velocity and pressure. The placement of the first grid point was established on the basis of the non-dimensional distance parameter  $y^+$ , describing local Reynolds number. For the first estimation,  $y^+$  may be determined

according to the theory of flat-plate flow, e.g. Schlichting (1968)

$$y^+ = 0.172 \left( \frac{y}{L} \right) R_n^{0.9} \quad (3.3)$$

where  $y$  is the distance from the wall,  $L$  is the body length. Wall functions have been applied in the considered case, maintaining  $y^+ = 50$ . Calculations were carried out for the Reynolds number of the model keeping the Froude number similarity. The scale factor was  $\lambda = 30$ . The shape of computational domain, presented in Fig. 4, was designed intentionally for the purpose of changing the velocity vector direction at the inlet boundary condition. The outer boundary is a surface of revolution created by the revolution of a trapezoid placed at the waterline.

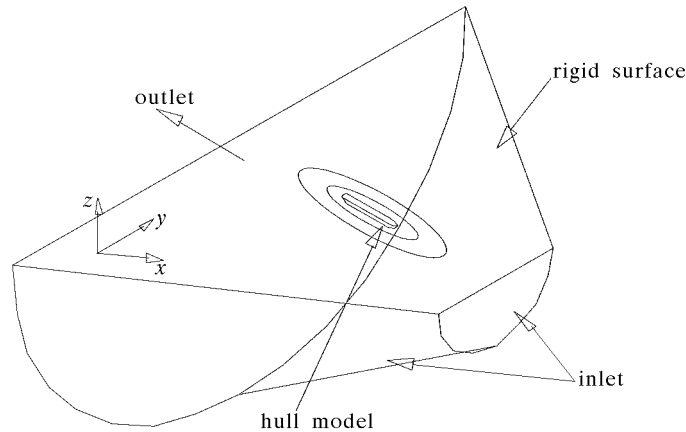


Fig. 4. The shape of computational domain

Four types of boundary conditions were placed at the outer surfaces of computational domain:

- The free surface was replaced with a rigid boundary and is treated as a rigid plane of symmetry, for which conditions of zero normal velocity and zero gradient of other components must be satisfied. This, of course, implies neglecting of free surface effects. This assumption may be legitimate taking into account that the Froude number is relatively low ( $Fn = 0.16$ ). The flow around a hull with a high block coefficient and relative velocity lowered to  $Fn = 0.16 - 0.17$  is much more affected by viscosity than wave making effects (Zborowski, 1980).
- The boundary condition on the hull is a no-slip condition with zero relative speed enforced.

- At the inlet boundary condition, all flow parameters must be specified. Components of the free stream velocity vector have been changed following the scope of the drift angle

$$V_x = -V \cos \beta \quad V_y = -V \sin \beta \quad (3.4)$$

where  $\beta$  is the drift angle and  $V$  is the model velocity. Turbulence parameters have been given according to the approach of the turbulence intensity  $I$  and reference length  $l$ , as the RNG  $k - \varepsilon$  model was applied. The kinetic energy  $k$  was calculated as

$$k = \frac{3}{2}(VI)^2 \quad (3.5)$$

The dissipation rate  $\varepsilon$  is

$$\varepsilon = 0.164 \frac{k^{1.5}}{l} \quad (3.6)$$

- The outlet condition was set to ensure that longitudinal gradients of velocity and pressure are equal to zero

$$\frac{\partial(u, v, w, p)}{\partial x} = 0 \quad (3.7)$$

Arrangement of boundary conditions is presented in Fig. 4. The change of the drift angle was done by modification of velocity components at the inlet condition. The flow was computed for drift angles varying from  $0^\circ$  to  $35^\circ$ , with step by  $5^\circ$ . The hull of a bulk carrier has been chosen for the analysis. Parameters of a ship hull together with flow numbers are presented in Table 3. A sketch of body lines is given in Fig. 5.

**Table 3.** Parameters of a ship hull

Parameters	ship	model
Length, $L$ [m]	185	6.167
Breadth, $B$ [m]	25.3	0.843
Draught, $T$ [m]	10.65m	0.355
Block coefficient, $C_B$	0.815	0.815
Speed, $V$	14 w	1.315 m/s
Froude number, $Fn$	0.16	0.16
Reynolds number, $Re$	$1.4 \cdot 10^9$	$6.8 \cdot 10^6$

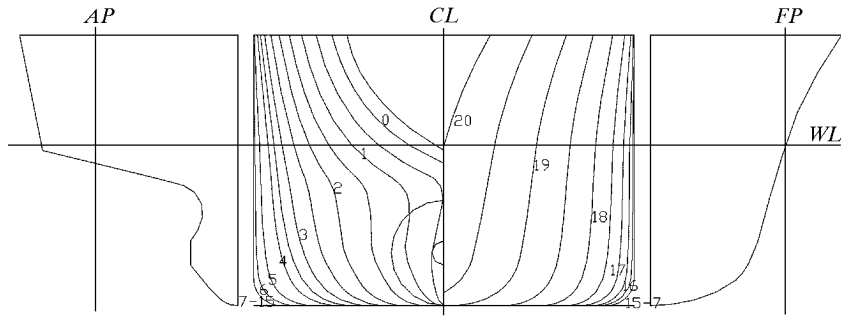


Fig. 5. Bulk carrier body lines

An unstructured hybrid grid with tetrahedral elements placed in the most part of the domain and prismatic elements near the hull has been applied for discretization. The grid topology is presented in Fig. 6 (view from the bottom and stern part). The total number of elements was 680000.

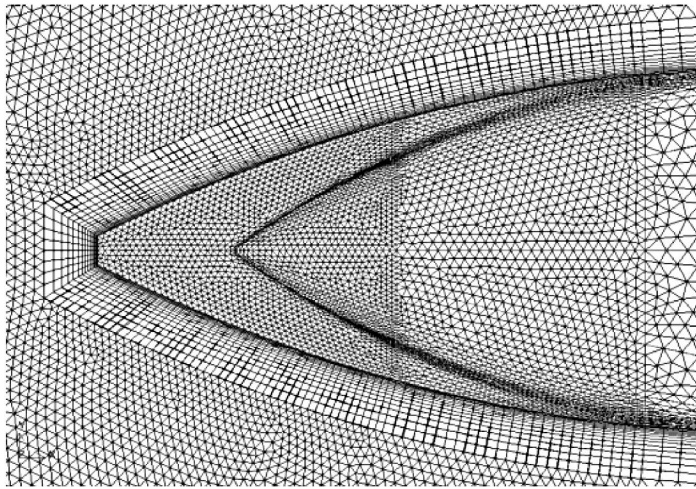


Fig. 6. View of the numerical grid in the stern region

The results show complex features of the flow in the stern region. Streamlines are presented in Fig. 7 and Fig. 8, in the stern view. Formations of strong vortices are present, even for the straight ahead course case. The convergence was ensured on the basis of the solutions history for drag and lift forces, see Fig. 10 and Fig. 11. Distributions of the nominal wake factor  $w_N$  are calculated according to Taylor's approach

$$w_N = 1 - \frac{V_{AX}}{V_X} \quad (3.8)$$

where  $V_{AX}$  is the axial component of the velocity in the screw plane,  $V_X$  is the axial component of ship's speed.

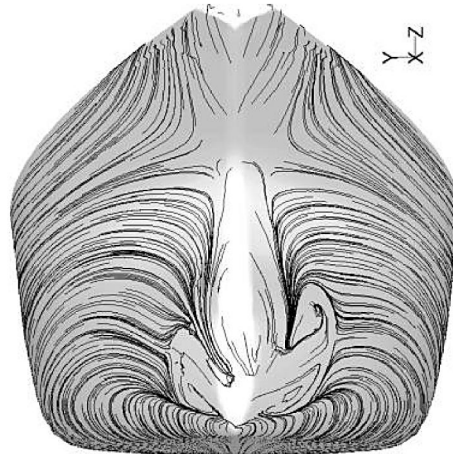


Fig. 7. Calculated streamlines for  $\beta = 0^\circ$ . A view from the stern of the ship

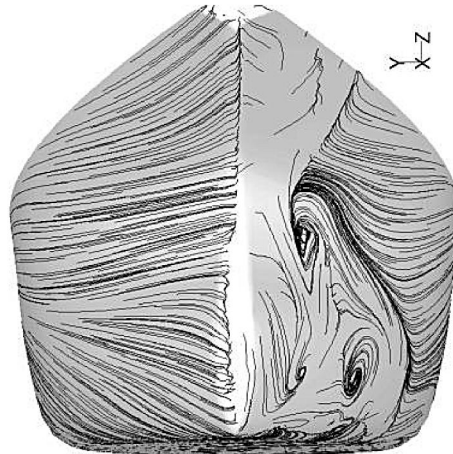


Fig. 8. Calculated streamlines for  $\beta = 35^\circ$ . A view from the stern of the ship

The wake is strongly non-uniform both in radial and circumferential directions, and the non-uniformity is stronger as the drift angle increases. The flow straightening effect of the hull causes strong non-uniformity of the wake, which becomes visible in regions where backflow occurs. Mean values of the wake factor decrease when the drift angle gets higher, Fig. 9. Mean values

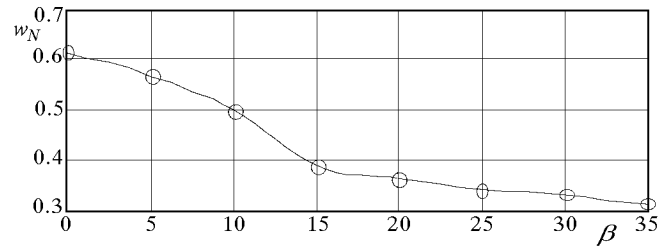


Fig. 9. Mean values of the nominal wake factor

of the wake factor presented there were calculated on the basis of its radial distribution, defined as

$$w_N(r) = \frac{1}{360} \int_0^{360} w_N(\varphi) d\varphi \quad (3.9)$$

where  $r$  is the assumed radius of screw and  $\varphi$  is the circumferential position. Hence, the mean value of the wake factor was determined as

$$w_N = \frac{1}{0.48} \int_{0.2}^1 r w_N(r) dr \quad (3.10)$$

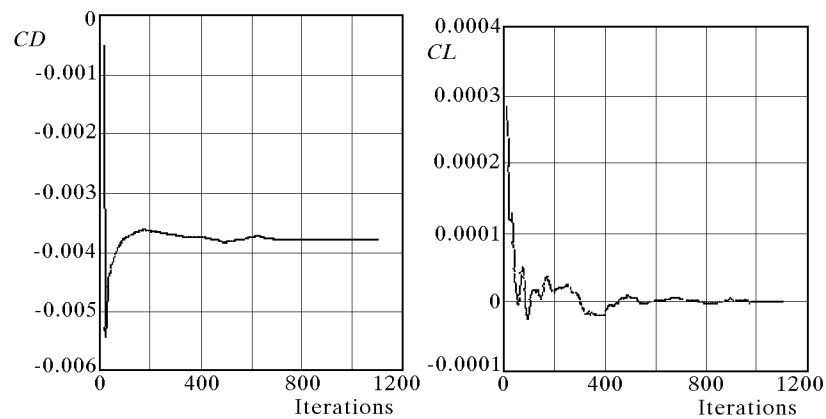


Fig. 10. Convergence history of drag and lift forces. Drift angle  $\beta = 0^\circ$

Unfortunately, we did not have any experimental results of the wake and streamlines for a reliable verification process. Furthermore, because we have neglected free surface effects, then comparison of values for the total resistance

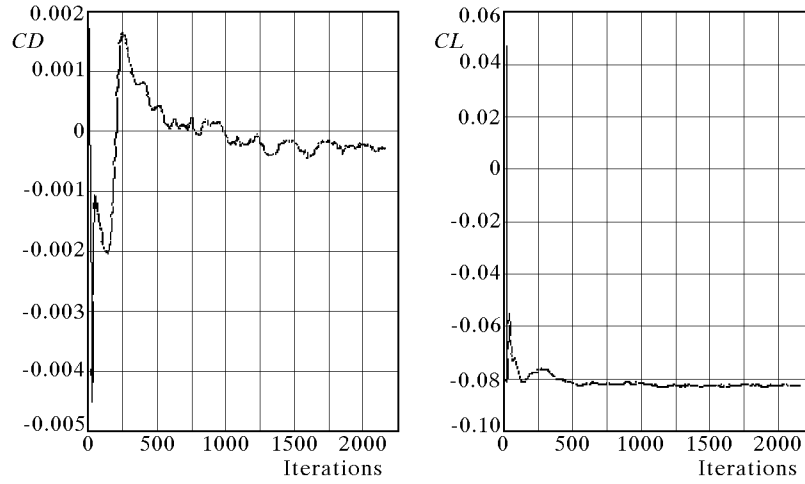


Fig. 11. Convergence history of drag and lift forces. Drift angle  $\beta = 35^\circ$

might be difficult to review. We have attempted to assess the results for the straight ahead course case, related to the viscous part of the total resistance. According to Froude's hypothesis, the hull resistance can be divided into its viscous and residual parts

$$C_T = C_R + C_V \quad (3.11)$$

where  $C_T$  is the total resistance coefficient,  $C_R$  is the residual resistance coefficient,  $C_V$  is the viscous resistance coefficient. The viscous coefficient is a function of the Reynolds number and the shape of a ship. It can be expressed as

$$C_V = (1 + k_0)C_{F0} \quad (3.12)$$

where  $k_0$  is the form factor, and  $C_{F0}$  is the frictional resistance coefficient. The frictional resistance coefficient can be estimated by means of the ITTC (International Towing Tank Conference) friction line

$$C_{F0} = \frac{0.075}{(\log(Re) - 2)^2} \quad (3.13)$$

The form factor  $k$  was estimated according to the following empirical formula (Dudziak, 1988)

$$k_0 = 0.017 + 20 \frac{C_B}{\left(\frac{L_W}{B}\right)^2 \sqrt{\frac{B}{T}}} \quad (3.14)$$

where  $C_B$  is the ship block coefficient and  $L_W$  is the waterline length. The numerical algorithm calculates hydrodynamic forces by integration of normal

pressure stresses and frictional shear stresses over the hull surface. The total resistance coefficient can be expressed as a sum of these components

$$C_x = C_{px} + C_{fx} \quad (3.15)$$

where  $C_{px}$  is the pressure induced resistance coefficient and  $C_{fx}$  is the frictional resistance coefficient. The negligence of the free surface effect implies that the residual coefficient  $C_R$  in Eq. (3.11) can be assumed to be equal to zero. The pressure coefficient  $C_{px}$  expresses the form resistance of the hull, and it is possible to use it for calculation of the form factor  $k_0$ .  $C_{fx}$  can be compared with the ITTC formula. Hence, Eq. (3.11) can be written as

$$C_T = k_0 C_{F0} + C_{F0} \quad (3.16)$$

By comparison between Eq. (3.16) and Eq. (3.15),  $k_0$  can be written as

$$k_0 = \frac{C_{px}}{C_{fx}} \quad (3.17)$$

The results of calculations presented above are shown in Table 4.

**Table 4.** Resistance coefficients

	$C_{fx}$	$C_{px}$	$C_x$	$1 + k_0$
Calculations	$2.98 \cdot 10^{-3}$	$0.745 \cdot 10^{-3}$	$3.73 \cdot 10^{-3}$	1.25
ITTC	$3.21 \cdot 10^{-3}$	–	–	1.37

#### 4. Application of wake calculation results to prediction of propeller forces during ship turning circle maneuver

The results of numerical calculations of the nominal wake of a ship moving with drift may be used as an input for the determination of propeller forces and torque. A simple example of such application for a ship performing the turning circle maneuver is presented in this section. Having calculated the propeller characteristics and nominal wake factor  $w_N$ , we must further take the propeller action into consideration in order to calculate the effective wake factor  $w$ . The effective wake factor can be directly put into Eqs. (1.1) and (1.2). The following formulation of a function describing the effective wake was assumed

$$w = f[w_N(\beta); C_{Th}(K_T, J); \delta] \quad (4.1)$$

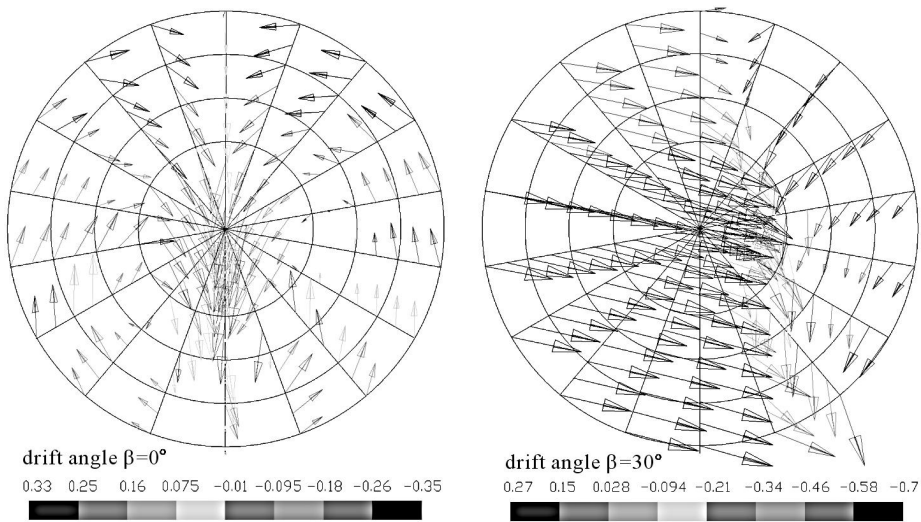


Fig. 12. Transverse velocities in the propeller plane;  $V_Y$  [m/s]

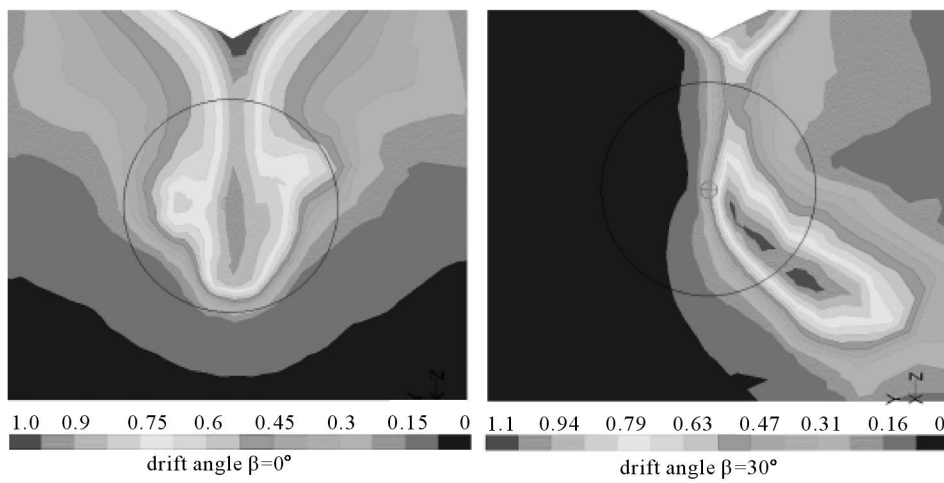


Fig. 13. Wakes distributions in the propeller plane

In the above equation,  $C_{Th}$  is the thrust loading coefficient of the propeller running behind the hull

$$C_{Th} = \frac{8}{\pi} \frac{K_T}{J(w)^2} \tag{4.2}$$

where  $J$  is the advance coefficient as in Eq. (1.2),  $K_T$  is the thrust coefficient and  $\delta$  is the rudder angle. The formula proposed by Pustoshny and Titov (1980), based on the actuator disc theory and some model test results, was

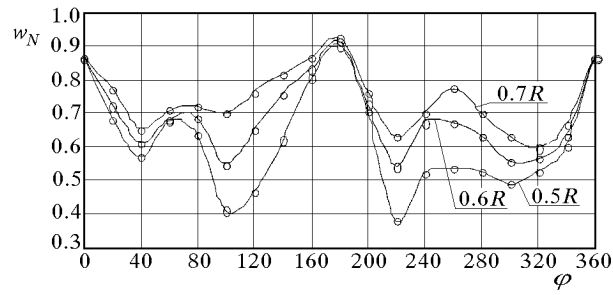


Fig. 14. Circumferential distribution of the wake factor. Drift angle  $\beta = 0^\circ$

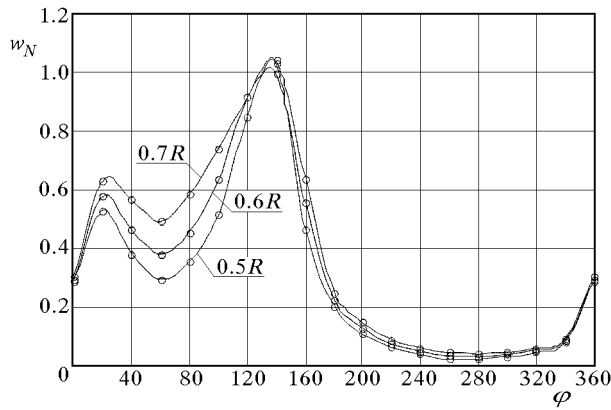


Fig. 15. Circumferential distribution of the wake factor. Drift angle  $\beta = 35^\circ$

applied for the transformation of the nominal wake  $w_N$  into the effective wake factor  $w$ , which can be done by the following formula

$$w = \frac{w_N \sqrt{2}}{\sqrt{1 + \sqrt{1 + C_{Th}(w)}}} \quad (4.3)$$

The above non-linear equation was solved by iteration. Furthermore, the effect of the rudder angle  $\delta$  on the effective wake was considered on the basis of model test results for a ship moving straight ahead, presented by Simonsen (2000). For the sake of simplicity, the results presented there were approximated in the analysis by a second degree polynomial

$$\frac{w_\delta}{w} = 0.0001\delta^2 - 0.0013\delta + 1 \quad (4.4)$$

where  $w_\delta$  is the effective wake factor for a given rudder angle and  $w$  is the effective wake factor for  $\delta = 0^\circ$ . The calculations were carried out for the

turning circle maneuver performed by a bulk carrier ship. The initial ship speed was 14 knots, which corresponds to the engine setting "full-ahead" for the analyzed case. The results presented in Fig. 16 and Fig. 17, show noticeable changes of all calculated coefficients during the maneuver.

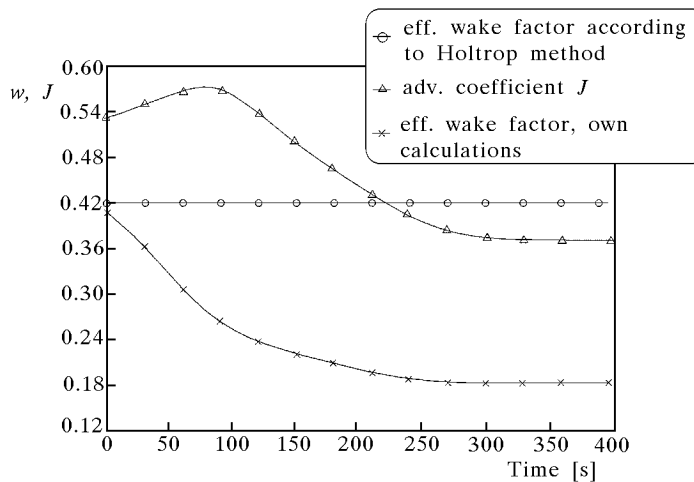


Fig. 16. Changes of the effective wake factor and the advance coefficient during the turning circle maneuver. Values of the effective wake factor were compared against the Holtrop method

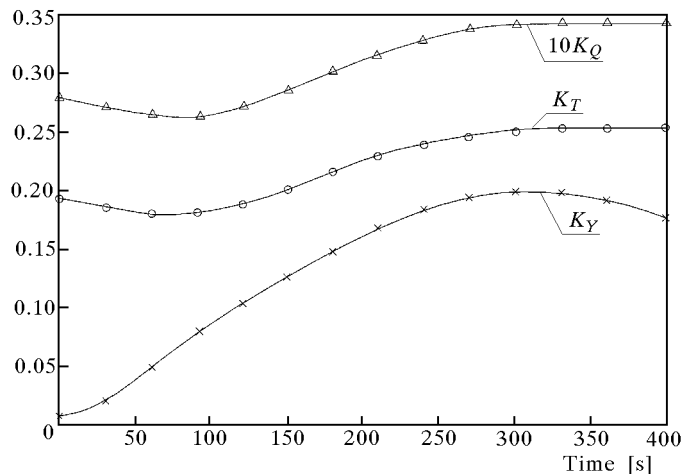


Fig. 17. Calculated changes of thrust, torque and side force coefficients

The obtained value of the effective wake factor at the beginning of the maneuver (straight ahead course) was 0.4. The same value calculated by means

of the widely applied Holtrop method was 0.41. It can be seen in Fig. 16, how much the wake coefficient calculated by the presented method differs from that calculated by the method not taking into account the oblique inflow, when the drift angle was getting higher during the course of the maneuver.

## 5. Final remarks

The method presented in the paper can be applied in numerical maneuvering simulators and for the assessment of propeller performance working under above assumed conditions. Artificial neural networks used for the prediction of the four-quadrant propeller performance showed good correlation with experimental data. They seem to be a promising tool for practical use. The case of a ship moving with drift causes complicated flow patterns in the stern region. Thus, for the purpose of carrying out such calculations, it is clearly needed to apply most advanced numerical techniques, taking real hydrodynamics effects into consideration. The RANS viscous method has been applied here and the results were at least qualitative for mean and integral values. Inaccuracies may come from imperfections of the applied turbulence model and its consequences as well as from errors introduced by the numerical method. The results obtained for streamlines in the stern region are especially interesting, where complicated vortex formations can be observed. The assumption neglecting free surface effects seems to be legitimate in the assumed range of the Froude flow number and for the assumed purpose of calculations, which was the investigation of the wake factor. If the aim of analysis was to calculate hull forces, better accuracy would be advisable. The results of flow calculations can be applied an algorithm for the determination of screw propeller forces in maneuvering conditions, and an example of such an application was briefly discussed.

## References

1. ABRAMOWSKI T., 2003, Numeryczne określanie sił i momentu śruby napędowej manewrującego statku na wodzie spokojnej z prądem powierzchniowym, Rozprawa Doktorska, Politechnika Szczecińska WTM Szczecin
2. BASIN A.M., MINIOVICH I.YA., 1963, *Teorya i Razchet Grebnykh Vintov*, Sudprom

3. BERTRAM V., 2000, *Practical Ship Hydrodynamics*, Butterworth-Heinemann
4. CARLTON J.S., 1994, *Marine Propellers and Propulsion*, Butterworth-Heinemann
5. CHEN B., STERN F., 1999, Computational fluid dynamics of four-quadrant marine-propulsor flow, *Journal of Ship Research*, **43**, 4, 218-228
6. DUDZIAK J., 1988, *Teoria okrętu*, WM Gdańsk
7. EL MOCTAR O.M., 2001, Numerical computations of flow forces in ship maneuvering, *Ship Technology Research*, **48**, 98-123
8. FERZIGER J.H., PERIC M., 2002, *Computational Methods for Fluid Dynamics*, Springer-Verlag
9. FUJINO M., 1996, Prediction of ship maneuverability: State of the art, *Int. Conf. On Marine Simulation and Ship Manoeuvrability*, Rotterdam, 371-387
10. GRYBOŚ R., 1998, *Podstawy mechaniki płynów*, PWN, Warszawa
11. INOUE S., HIRANO M., KIJIMA K., TAKASHINA J., 1981, A practical calculation method of ship maneuvering motion, *Int. Shipbuilding Progress*, **28**, 207-222
12. JARZYNA H., 1993, *Wzajemne oddziaływanie kadłuba i pędnika statku*, MP tom 14, Ossolineum i Wydawnictwo PAN
13. JARZYNA H., KORONOWICZ T., SZANTYR J., 1996, *Design of Marine Propellers*, MP tom 20, Ossolineum i Wydawnictwo PAN
14. KIJAMA K., TANAKA S., FURUKAWA Y., HORI T., 1993, On a prediction method of ship manoeuvring characteristics, *Int. Conf. on Marine Simulation and Ship Manoeuvrability*, St. John's, 285-294
15. KOBYLIŃSKI L., ZOLFAGHARI G., 1997, Prediction of manoeuvring characteristics in ship design, *12th Int. Conf. Hydrodynamics in Ship Design*, Szklarska Poręba, 197-209
16. KOUSHAN, K., 2000, Prediction of propeller induced pressure pulses using artificial neural networks, *1st Int. Conf. Computer Applications and Information Technology in the Maritime Industries*, Potsdam
17. LAM S.H., 1992, On the RNG theory of turbulence, Department of Mechanical and Aerospace Engineering, Princeton University, Princeton, NJ 08544-5263, *Physics of Fluids A*, **4**, 1007-1017
18. KROSE B., SMAGT P.V.D., 1996, *An Introduction to Neural Networks*, The University of Amsterdam
19. LAMMEREN W.P.A., MANEN J.D., OOSTERVELD M.W.C., 1969, The Wageningen B-screw series, *Trans. SNAME*, 269-288

20. LE THUY HANG, 2001, Calculation of the influence of propeller operation on the hydrodynamic characteristics of the rudder, *Polish Maritime Research*, **8**, 2(28), 3-9
21. MESBAHI E., ATLAR M., 2000, Artificial neural networks: applications in marine design and modelling, *1st Int. Conf. Computer Applications and Information Technology in the Maritime Industries*, Potsdam
22. OSOWSKI S., 1996, *Sieci neuronowe w ujęciu algorytmicznym*, WNT
23. PUSTOSHNY A.F. TITOV I.A., 1980, *Sbornik statei po gidrodinamike transportnykh sudov*, KRSI
24. SCHLICHTING H., 1968, *Boundary Layer Theory*, McGraw-Hill, New York
25. SIMONSEN C.D., 2000, Rudder, Propeller and hull interaction by RANS, PhD Thesis, T.U. of Denmark
26. WELNICKI W., 1966, *Sterowność okrętu*, PWN, Warszawa
27. YASUKAWA H., YOSHIMURA Y., NAKATAKE K., 1996, Hydrodynamic forces on a ship with constant rudder angle: a theoretical treatment of rudder angle test, *Int. Conf. On Marine Simulation and Ship Manoeuvrability*, Rotterdam, 435-447
28. ZBOROWSKI A., 1980, *Opór statków wypornościowych*, WM, Gdańsk

### **Określanie sił śruby napędowej podczas manewrowania statkiem**

#### Streszczenie

W pracy zaproponowano metodę służącą do określenia sił śruby napędowej podczas manewrowania statkiem. Do wyznaczenia charakterystyk śruby napędowej pracującej w warunkach hamowania, zatrzymywania i ruchu wstecz zastosowano sztuczne sieci neuronowe. Ponadto, przy pomocy metod numerycznej mechaniki płynów uwzględniono efekt skośnego ruchu kadłuba manewrującego statku. Zaprezentowano obliczone podczas zwiększania się kąta dryfu rozkłady strumienia nadążającego w płaszczyźnie kręgu śrubowego. W oparciu o prosty przykład przedyskutowano możliwość zastosowania zaprezentowanej metody dla rzeczywistego przypadku manewrującego statku.

*Manuscript received March 29, 2004; accepted for print May 10, 2004*